A novel glucose sensor using lutetium phthalocyanine as redox mediator in reduced graphene oxide conducting polymer multifunctional hydrogel

AL-SAGUR, H, KOMATHI, S, KHAN, M, GUREK, A G and HASSAN, Aseel <http://orcid.org/0000-0002-7891-8087>

A novel glucose sensor using lutetium phthalocyanine as redox mediator in reduced graphene oxide conducting polymer multifunctional hydrogel

H. Al-Sagur[1†], S. Komathi[1†], M. A. Khan[2], A.G Gurek[3] and A. Hassan[1]*
[1]Materials and Engineering Research Institute, Sheffield Hallam University, Sheffield, UK
[2]Biomedical Research Institute, Sheffield Hallam University, Sheffield, UK
[3]Gebze Technical University, Department of Chemistry, Gebze 41400, Kocaeli, Turkey

*† authors contributed equally, * corresponding author*

Abstract

Herein, we report a scalable synthesis of multifunctional conducting polyacrylic acid (PAA) hydrogel (MFH) integrated with reduced grapheme oxide (rGO), vinyl substituted polyaniline (VS-PANI) and lutetium Phthalocyanine ($LuPc_2$) as three dimensional robust matrix for glucose oxidase (GOx) immobilization (PAA-rGO/VS-PANI/$LuPc_2$/GOx-MFH). We have integrated the multicomponents such as PAA with rGO, and VS-PANI through free radical polymerization using methylene bis-acrylamide, and ammonium persulphate as the cross linker and initiator. The $LuPc_2$ was then doped to form multifunctional hydrogel (PAA-rGO/VS-PANI/$LuPc_2$-MFH). Finally, biosensor was fabricated by immobilizing GOx into PAA-rGO/VS-PANI/$LuPc_2$-MFH and subsequently used for electrochemical detection of glucose. The PAA-rGO/VS-PANI/$LuPc_2$/GOx-MFH biosensor exhibited high sensitivity (15.31 $\mu AmM^{-1}cm^{-2}$) for the detection of glucose over a concentration range of 2–12 mM with a low detection limit of 25 μM. The PAA-rGO/VS-PANI/$LuPc_2$-MFH biosensor showed a fast response time (1s) to the addition of glucose with high storage stability of 3 months. The real sample analysis reveals that PAA-rGO/VS-PANI/$LuPc_2$/GOx-MFH could be effectively used as an electrochemical biosensor in industrial as well clinical diagnosis.

Keywords: Polyacrylic acid, reduced graphene oxide, polyaniline, lutetium Phthalocyanine, glucose biosensor, multifunctional hydrogel

1. Introduction

Despite many technological advances in biosensor research, the worldwide increase in the prevalence of chronic disease (diabetes mellitus) has been the driving force for the development of glucose sensors (Wang and Lee, 2015). Diabetes, occurs due to malfunctioning of pancreatic β cells responsible for production of insulin that control glucose level in the blood (Schuit et al., 2001). About 5 percent of the world's population (3.9 million people in the UK alone) are living with diabetes (Diabetes UK, 2015). The elevated level of glucose (normal range 4.4–6.6 mM) poses serious health problems in diabetic patients and accounts for 4 million deaths worldwide every year (Wild, et al, 2014). Frequent self-monitoring of glucose may provide data for optimizing and/or changing insulin uptake in patients (Canadian Diabetes Association, 2008).

Although several conventional methods available for the detection of glucose, electrochemical detection of glucose show unique advantages such as fast response, sensitive, low cost and does not require skilled labour or large instrumentation for detection (Rahman et al., 2010). Non enzymatic electrochemical sensors exhibit poor performance in selectivity and suffer from interference from electrochemically active molecules (Toghill and Compton, 2010). Glucose oxidase (GOx) is the widely studied enzyme for amperometric glucose sensing since its inception from Clark and Lyons in 1962 (Claussen et al., 2012; Wang 2001). The key factor for an efficient GOx based sensor is to obtain electron transfer from the active centre, flavin adenine dinucleotide (FAD) enwrapped within thick protein layer, maintain biological activity, high enzyme loading and avert enzyme leeching. Additionally, an ideal biosensor has to be stable for long-term application, accurate in sensor-to-sensor measurements with significant operational lifetimes. To achieve these factors, large number of substrates as recognition elements such as carbon nanotubes (Zhu et al., 2012), graphene (Unnikrishnan et al., 2013), inorganic nanostructures (Wu et al., 2015), conductive polymers (Chen et al., 2006; Garjonyte and Malinauskas, 1999), cellulose acetate (Ren et al., 2009), polyacrylonitrile (Zheng et al, 2002) have been proposed for GOx immobilization. However fewer reports are available on the utilization of a robust three dimensional multifunctional conducting hydrogel as an enzyme immobilization matrix and subsequent biosensing of glucose.

Hydrogels are physically or chemically three-dimensional cross-linked, insoluble hydrophilic polymeric network with the capability to swell in the presence of aqueous

solution or biological fluids (Barakat and Sahiner, 2008; Sezgin and Balkaya, 2015). Hydrogel networks formed from polyacrylic acid (PAA) have the ability to absorb more than hundred times their weight in water and they are classified as super absorbents (Dhodapkar et al., 2009). PAA hydrogel plays an important role as pH stimuli-responsiveness and bioadhesive characteristics because of the presence of −COOH groups in their chain (Arunbabu et al., 2013). However, pristine polymeric hydrogels are mechanically weak and poses insufficient electrical conductivity that limits their application as electrochemical sensors (Damia Mawad, 2016). The incorporation of nanomaterials into robust hydrogels generates tailored functionalities feasible to construct sensor and other drug delivery vehicles (Puoci and Curcio, 2013; Gaharwar et al., 2014). Especially, integration of graphene with polymeric hydrogel offer enhanced actuation performance due to its excellent physico-mechanical properties and facile conjugation reactions (Worsley et al., 2012; Bhattacharjee et al., 2013). The presence of hydroxyl, epoxy and carboxyl end functional groups on the surface of GO provide multiple conjugation avenue and endow electrochemical properties to hydrogel matrices (Bai et al., 2010; Liu et al., 2011).

PANI based conducting hydrogels that combine the properties of both conducting polymers and hydrogels, find potential application in the fields of electrochemical energy storage, metal corrosion resistance, biological and chemical sensor (Guo et al., 2015; Wang et al., 2014; Nath et al., 2014; Ding et al., 2015). The inbuilt properties of hydrogels such as good biocompatibility and permeability to water-soluble biochemicals in combination with excellent electronic properties of PANI would be an ideal matrix for enzyme immobilization and preserves their bioactivity for electrochemical detection. Moreover, the 3D conducting polymer network offers sufficient charge collection capacity to hydrogel. Overall the synthetic method can be easily manipulated to construct intricately patterned electrodes at low cost (Heller, 2006; Åsberg and Inganäs, 2003). Pan et al (2012) have reported on the synthesis of hierarchical nanostructured PANI hydrogel, in which phytic acid is used as the gelator and dopant to directly form a conducting polymer network. Here we propose vinyl substituted polyanine (VS-PANI) forming hydrogel in the presence of PAA.

Metallophthalocyanines (MPc) show good electrocatalysis in the oxidation of several industrially and biologically important molecules (Barrera et al., 2006; Pereira-Rodrigues et al., 2002). d-block MPc (Fe, Co) complexes with macrocyclic extended π-systems endow them to undergo fast redox processes with minimal reorganizational energies have been intensively studied as redox mediators for glucose enzyme electrodes (Hart and Wring,

1997; Wang et al., 2005). GOx catalyses the oxidation of glucose, in which the natural electron-acceptor (oxygen) is converted to the H_2O_2. Modification of the electrode surface with highly biocompatible MPc will reduce the voltage requirement for H_2O_2 oxidation (Ozoemena et al., 2005). Among numerous MPc families, double-decker lanthanide derivatives, lutetium phthalocyanine ($LuPc_2$) attract interest due to their high intrinsic conductivity and electrochemical properties (Basova et al., 2008). The electrochromic behaviour of lanthanide phthalocyanine films has been used for the detection of nicotinamide adenine dinucleotide (Pal et al., 2011; Galanin and Shaposhnikov, 2012a). Synthesis and spectral properties of lanthanide double-decker complexes with tetrabenzoporphyrin and phthalocyanine have also been studied (Galanin and Shaposhnikov, 2012b).

Herein, we report a scalable synthesis of multifunctional conducting PAA hydrogel (MFH) integrated with rGO, VS-PANI and $LuPc_2$ as three dimensional robust matrix for GOx immobilization (PAA-rGO/VS-PANI/$LuPc_2$/GOx-MFH). We have integrated the multicomponents such as PAA with rGO, VS-PANI through free radical polymerization using methylene bis-acrylamide as the cross linker and initiator. The $LuPc_2$ was then doped to form multifunctional hydrogel (PAA-rGO/VS-PANI/$LuPc_2$-MFH). Finally, biosensor was fabricated by immobilizing GOx into PAA-rGO/VS-PANI/$LuPc_2$-MFH and subsequently used for electrochemical detection of glucose.

2. Experimental

2.1. Chemicals

rGO (surface area: 450 m^2/g), poly(ethylene glycol) diamine (NH_2-PEG-NH_2), *N*-(3-dimethylaminopropyl)-*N*′-ethylcarbodiimide hydrochloride (EDC hydrochloride), acrylic acid, 3-vinylaniline (97%), N,N′-methylenebis(acrylamide) (MBA), ammonium persulfate (APS), D-(+)glucose, glucose oxidase from aspergillus niger, Type X-S, lyophilized powder, 100,000-250,000 units/g solid (without added oxygen), glutaraldehyde solution (Grade II, 25% in H_2O), Potassium ferrocyanide, Potassium ferricyanide, potassium chloride (KCl), sodium chloride (NaCl), phosphate buffer solution (PBS, pH 7.0) were all purchased from Sigma Aldrich (UK) and used as received. Synthesis and characterisation of lutetium bis-phthalocyanine ($LuPc_2$) has appeared in an earlier publication (Gurek et al., 2001). *N*,*N*-Dimethylformamide (DMF) is of analytical grade obtained from Sigma Aldrich.

2.2. Apparatus

The morphologies of the prepared MFH were examined by FEI-Nova scanning electron microscopy (SEM) with a low magnification (160,000×) and high voltage (10 kV). UV–Visible spectrophotometer (Varian 50-scan UV–Visible) in the range 190–1100 nm was used to measure the absorption spectra of MFH. FT-IR spectra were recorded on a Perkin Elmer Spectrum 100 spectrophotometer. The electrochemical measurements of the electrodes were conducted using a portable bipotentiostats μStat 200 that was purchased from DropSens (Spain) and controlled by PC with DropView 200 software. The sensor platforms were disposable screen-printed carbon electrodes DRP-C110 also from DropSens with 4 mm diameter working electrode. The working and auxiliary electrodes are carbon, while silver forms the reference electrode and the träger (carrier) is ceramic. The working electrodes were modified with PAA-rGO/VS-PANI/$LuPc_2$/GOx-MFH or PAA-VS-PANI/$LuPc_2$/GOx-MFH or PAA-$LuPc_2$/GOx-MFH. The electroactivity of MFH modified electrode was evaluated by recording cyclic voltammogram in potassium ferro/ferricyanide solution containing 0.1 M NaCl in the potential range from -0.5V to +0.5V. The biocatalytic activity of PAA-rGO/VS-PANI/$LuPc_2$/GOx-MFH biosensor was evaluated by cyclic voltammetry for a solution of 4 mM glucose in 0.1 M PBS. The amperometric responses of PAA-rGO/VS-PANI/$LuPc_2$/GOx-MFH biosensor towards glucose detection were recorded under stirred conditions in 0.1 M PBS (pH 7.0) by applying a constant potential of +0.3 V at the working electrode.

2.3. Preparation of PAA-rGO/VS-PANI/$LuPc_2$/GOx-MFH biosensor

The preparation of MFH involves three steps: (i) preparation of amine functionalized rGO, (ii) formation of PAA-rGO/VS-PANI-MFH, (iii) incorporation of $LuPc_2$ and subsequent immobilization of GOx to form PAA-rGO/VS-PANI/$LuPc_2$/GOx-MFH biosensor.

2.3.1. Preparation of amine functionalized rGO

Amine functionalized rGO preparation was carried out according to earlier reports (Lei et al., 2016). Briefly, about 10 mg of rGO was dispersed in 10 mL of water containing NH_2-PEG-NH_2 (0.1 g) and EDC.HCl (0.1 g) under vigorous stirring overnight. rGO-PEG-NH_2 thus obtained were allowed to settle down and filtered through polycarbonate membrane (pore size=200 nm). The samples were dried in vacuum oven at 60^{o}C for further use.

2.3.2. Formation of PAA-rGO/VS-PANI-MFH

5 mg of rGO-PEG-NH_2 was dispersed in 10 mL of HCl (0.1M) containing 10 mg of EDC.HCl under sonication. Subsequently, AA (2.4 mL), MBA (2 M) 3-vinylaniline (0.1 M) and APS (0.2 M) were added into the mixture with continued stirring. The above solution mixture was purged with N_2 gas to remove the dissolved oxygen content and poured into a pre-cleaned vial. The vial was placed in the vacuum oven maintained at 70 °C for about an hour. A solid hydrogel was formed at around 45 min. The solid hydrogel was cooled to room temperature. The colour of the hydrogel turned to green with black spots to form PAA-rGO/VS-PANI-MFH. For comparative purposes, PAA/VS-PANI-MFH and PAA-rGO-MFH were prepared separately. This was achieved by excluding rGO-PEG-NH_2 and 3-vinylaniline respectively in the hydrogel preparation step. It took around 90 min for gelation in the absence of rGO-PEG-NH_2 (PAA/VS-PANI-MFH) and 60 min in the absence of 3-vinylaniline (PAA-rGO-MFH). The hydrogels thus obtained were systematically analyzed by SEM, UV-visible, FTIR spectroscopy to determine the morphology and chemical structure of the hydrogels.

2.3.3. Fabrication of PAA-rGO/VS-PANI/$LuPc_2$/GOx-MFH biosensor

Initially PAA-rGO/VS-PANI-MFH (2 µl) was formed as detailed before on the surface of screen printed electrode (Area = 0.1256 cm_2). Then $LuPc_2$ (2 µl) (5 mg dissolved in 1 mL chloroform) was dropped and allowed to dry in oven at 60^{o}C for 2 h. The fabrication of PAA-rGO/VS-PANI/$LuPc_2$/GOx-MFH biosensor was achieved by immobilizing GOx (1 µl) (10 mg in 1 mL PBS (pH 7.0)) along with glutaraldehyde (1 µl) and dried at room temperature for further analysis. Similarly, the other two PAA/VS-PANI/Pc_2/GOx-MFH biosensor and PAA-rGO/$LuPc_2$/GOx-MFH biosensor were fabricated.

3. Results and Discussion

3.1. Synthesis of PAA-rGO/VS-PANI-MFH

The steps involved in the preparation of the PAA-rGO/VS-PANI/$LuPc_2$/GOx-MFH are illustrated as scheme in Fig. 1A. Initially rGO-PEG-NH_2 was obtained through covalent grafting of PEG diamine chains onto carboxyl sites in the surface of rGO sheets via amidation in aqueous media. PAA-rGO/VS-PANI-MFH was formed through free radical polymerization of AA along with rGO-PEG-NH_2 and 3-vinyl aniline in the presence of MBA and APS (Layek and Nandi, 2013) (Fig. 1A). The inclusions of rGO-PEG-NH_2 and VS-PANI in the hydrogel were aimed to improve the binding sites and favourable conditions for

loading $LuPc_2$ and GOx immobilization. PAA containing –COOH groups in MFH protect VS-PANI in its protonated form. Fig. 1B shows a photograph of the prepared PAA-rGO/VS-PANI-multifunctional hydrogel (MFH). This hydrogel exhibits green colour which is originated from the protonated and doped VS-PANI in MFH with dispersed black spots.

3.2. Morphology

Fig.1B(a and b) shows SEM images of PAA-rGO/VS-PANI-MFH and PAA/VS-PANI-MFH respectively. PAA-rGO/VS-PANI-MFH clearly showed randomly distributed micro porous 3D inter-linked network, due to the integration of the components involved (Fig. 1B(a)). The average pore diameter of PAA-rGO/VS-PANI-MFH was estimated to be approximately 7µm. Such 3D interconnected hierarchical porous structure offers greater effective surface areas for $LuPc_2$ and GOx immobilization. However, the PAA/VS-PANI-MFH showed a layered structure characterised with smooth surface and much smaller pore size as shown in Fig. 1B(b). This suggests that VS-PANI twists with the PAA component and fills up the existent voids in PAA/VS-PANI-MFH. Further, the surface area of the MFH was also studied through Brunauer, Emmett and Teller (BET) measurements. From the BET results, the surface area of PAA-rGO/VS-PANI-MFH, PAA-rGO-MFH are calculated to be 1.3653 ± 0.1416 m^2/g and 0.9794 ± 0.1095 m^2/g respectively. We presume that the harsh pretreatment process (degassing condition – 3 h at 120 deg C) before N_2 physisorption has induced a collapse of the pores structure of MFH (Iza et al., 2000). The surface area value is slightly lower than previously reported polyacrylamide–polyacrylic acid copolymer hydrogel (4.9 m^2/g) (Li et al., 2002).

3.3. UV visible analysis

UV-visible spectrum of pristine $LuPc_2$ and hydrogels decorated with $LuPc_2$ (PAA-rGO/VS-PANI/$LuPc_2$, PAA/VS-PANI/$LuPc_2$ and PAA-rGO/$LuPc_2$), were recorded by using Cary 50 UV-Visible Spectrophotometer (190-1100 nm), as shown in Fig. 2. Thin films of $LuPc_2$ and the hydrogels were formed on the surface of pre-cleaned glass substrate. Main absorption peaks derived from the measured absorption spectra are presented in Table 1 (Supporting Information (SI-1). Bis-phthalocyanine complex of $LuPc_2$ thin film exhibited characteristic UV-visible B and Q absorption bands. A strong N-band at 317 nm, Soret B band at 390 nm region and intense visible Q band of the macrocycles at 706 nm can be seen (Fig. 2inset) (Basova et al., 2008). Also two weak p-radical blue valence (BV)/ red valence (RV) related bands attributed to 2eg–a1u and 1eg–a1u transitions were observed at 510–580 (BV) and

930–970 nm (RV), as reported earlier (Nekelson et al., 2007; Zheng et al., 2015; Pushkarev et al., 2012). In the hydrogels that includes VS-PANI, PAA-rGO/VS-PANI/$LuPc_2$ and PAA/VS-PANI/$LuPc_2$ showed a shoulder peak around 430 nm corresponding to the benzenoid to quinoid transitions of backbone PANI structure (Fig 2a,b). Additionally the N band of $LuPc_2$ was coupled with π–π* absorption peak of VS-PANI. These results demonstrate the presence of interconnected networks of VS-PANI in the hydrogel formed (Ipek et al., 2014). The Q band was shifted bathochromically in the case of PAA-rGO/VS-PANI/$LuPc_2$ to 712 nm (Fig 2a), PAA-rGO/$LuPc_2$ to 718 nm (Fig 2c) and hypsochromically in the case of PAA/VS-PANI/$LuPc_2$ to 702 nm (Fig 2b). This reveals the perturbance in the electronic states of $LuPc_2$ in MFH due to the electron transfer from rGO to phthalocyanine ring which leads to the formation of π–π stacking interaction between them and thus lower the band gap. This ensures that the studied MFHs were well decorated with double-decker lutetium (III) phthalocyanine moieties (Mani et al., 2015).

3.4. FTIR anaysis

The FTIR spectra of PAA-rGO/VS-PANI-MFH, PAA/VS-PANI-MFH and PAA-rGO-MFH are shown in the SI-2. PAA-rGO/VS-PANI-MFH exhibited the main characteristic absorption peaks of PAA around 2900-3600 cm^{-1} (-OH stretching), 1700 cm^{-1} (C=O stretching) and VS-PANI around 1450 cm^{-1} (benzenoid rings), 1620 cm^{-1} (quinoid rings) (Kennedy and Ratner, 1995; Saravanan et al., 2006; Nabid et al., 2007) (SI-2a). The absence of 1180 cm^{-1} peak in PAA/VS-PANI/$LuPc_2$ (SI-2b) and the suppression of 1450 cm^{-1} absorption peak in PAA-rGO/$LuPc_2$ (SI-2c) can be noticed which illustrates the difference in structure among the three prepared MFH.

3.5. Electrochemical performance of modified electrodes

Cyclic voltammograms (CVs) were recorded for the PAA-rGO/VS-PANI/$LuPc_2$/GOx-MFH, PAA/VS-PANI/$LuPc_2$/GOx-MFH, and PAA-rGO/$LuPc_2$/GOx-MFH biosensor using 5 mM potassium ferro/ferricyanide solution containing 0.1M NaCl as the bench mark redox system in the potential range from +0.5 to -0.5 V at a scan rate of 0.025 Vs^{-1} , as shown in Fig. 3. CVs of MFH based biosensor showed well-defined reversible peaks corresponding to the Fe(II)/Fe(III) redox transition process. The efficacy of the electrode was compared in terms of anodic to cathodic peak potential separation (ΔEp = Epa-Epc) and using oxidation or reduction peak currents (I_{pa} or I_{pc}) of the $Fe(CN)_6^{3-/4-}$. The I_{pa} of PAA-rGO/VS-PANI/$LuPc_2$/GOx-MFH Fig. 3(a) was ~2.32 and ~6.38 times higher than those exhibited by

PAA/VS-PANI/LuPc$_2$/GOx-MFH Fig. 3(b) and PAA-rGO/LuPc$_2$/GOx-MFH biosensor Fig. 3(c). However the Ipa of PAA-rGO/VS-PANI/LuPc$_2$/GOx-MFH (14.55 μA) was typically lower than the pristine PAA-rGO/VS-PANI/LuPc$_2$-MFH (21.6 μA) Fig. 3(d) prepared in the absence of GOx. This ensures the effective immobilization of GOx onto PAA-rGO/VS-PANI/LuPc$_2$-MFH matrix (Hua et al., 2012). Furthermore the ΔEp value increased from 105 mV for the PAA-rGO/VS-PANI/LuPc$_2$/GOx-MFH to 240 mv for the PAA-rGO/LuPc$_2$/GOx-MFH. The results demonstrates that the presence of VS-PANI as interconnecting network in MFH augment electronic conductivity and promote faster electron transport kinetics at PAA-rGO/VS-PANI/LuPc$_2$/GOx-MFH (Dou et al., 2016; Gopalan et al., 2013). CVs of PAA-rGO/VS-PANI/LuPc$_2$/GOx-MFH were also recorded for different scan rates (10–100 mV/s) (SI-3). A plot of Ipa and Ipc were linearly proportional to square root υ, which indicates a diffusion controlled process of $Fe(CN)_6^{3-/4-}$ redox reaction at PAA-rGO/VS-PANI/LuPc$_2$/GOx-MFH (Mashazi et al., 2006). From the plot of Ipa versus $\upsilon^{1/2}$ a slope of 1.194×10^{-4} A $V^{-1/2}$ $s^{1/2}$ was obtained. For the diffusion controlled reversible process the electrochemical active surface area (A) was determined using Randles–Sevcik equation (Siswana et al., 2006). From the D value for $K_3[Fe(CN)_6] = 6.7 \times 10^{-6}$ cm^2 s^{-1} (Ye et al., 2005), and n = 1, the area ('A') of PAA-rGO/VS-PANI/LuPc$_2$/GOx-MFH was estimated to be 0.244 cm^2. The value of 'A' of PAA-rGO/VS-PANI/LuPc$_2$/GOx-MFH was found to be higher than that of the bare GCE (0.078 cm^2), GOx/PANI microtube/GCE (0.156 cm^2) (Zhang et al., 2015) and rGO-C60/GOx (0.12 cm^2) (Thirumalraj et al., 2015) respectively. It is understood that the high value of 'A' results from the porous structure of PAA-rGO/VS-PANI-MFH as seen in Fig. 1B(a). Furthermore, swelling ratio of PAA-rGO/VS-PANI-MFH is found to be approximately 3 and 1.4 times higher than PAA/VS-PANI -MFH and PAA-rGO-MFH respectively at a fixed time. The higher swelling ratio value results from more pore volume at PAA-rGO/VS-PANI-MFH, where the larger the pore volume leads to lower diffusional resistance.

3.6. Electrochemical impedance measurements

The electrochemical surface characteristics of the electrodes modified with PAA-rGO/VS-PANI/LuPc$_2$/GOx-MFH (a) and PAA/VS-PANI/LuPc$_2$/GOx-MFH (b) were monitored through electrochemical impedance measurements in PBS containing 0.1M NaCl [SI-4A]. The immobilization of GOx enzyme onto the porous sites of the hydrogel alters the interfacial capacitance and electron-transfer resistance of the conductive electrodes (Ding et al., 2005;

Katz and Willner 2003; Pei et al., 2001). The nyquist plot of PAA-rGO/VS-PANI/$LuPc_2$/GOx-MFH biosensor (a) exhibited a much smaller semicircular diameter ascribed to electron-transfer resistance than those observed on PAA/VS-PANI/$LuPc_2$/GOx-MFH (b). The smaller semicircular diameter indicated faster electron transfer kinetics at high frequency region and the linear part at lower frequency region ensures mixed kinetics and diffusion controlled process. The lower charge transfer resistance (R_{ct}) for PAA-rGO/VS-PANI/LuPc2/GOx-MFH biosensor arises from the inter-connected PAA-rGO/VS-PANI network. The $LuPc_2$ decorated inside PAA-rGO/VS-PANI MFH provides easy electron conduction pathways. The impedance spectra obtained were fitted by a simple Randle circuit made up of electrolyte resistance (R_s), electron transfer resistance (R_{et}), double layer capacitance (C_{dl}) and Warburg coefficient (W). Data fitting was carried out using THALES software with a complex non-linear least-squares method. The equivalent circuit model is presented in [SI-4B].

3.7. Electrochemical detection of glucose

Fig. 4A shows the CV of PAA-rGO/VS-PANI/$LuPc_2$/GOx-MFH biosensor Fig. 4A(red curve) in bare PBS (pH 7.0) and in the presence of glucose (4mM) Fig. 4A(black curve). At PAA-rGO/VS-PANI/$LuPc_2$/GOx-MFH a reversible redox peak which corresponds to Lu(II)Pc_2/ Lu(III)Pc_2 was observed at -0.05 V/0.1 V under our experimental conditions, and this result is similar to results reported by Kadish et al. (2001). In the latter reference only one reduction and oxidation peak of $Lu(Pc)_2$ have been reported in a cast film in aqueous media (0.5 M KCl). For further confirmation, CV was also recorded for PAA-rGO/VS-PANI/$LuPc_2$-MFH in the absence of GOx, where a sharp redox couple at -0.12/ 0.1 V was obtained under identical conditions (Fig. 4A inset). Fig. 4A (black curve) shows the electrocatalytic oxidation of glucose (4 mM) at PAA-rGO/VS-PANI/$LuPc_2$/GOx-MFH. With the addition of glucose a large increase in anodic current, starting above 0.2 V was observed. This suggests that Lu(III)Pc_2 mediates electron transfer between the immobilized GOx and the electrode through oxidation of the reduced form of the enzyme. The plausible mechanism is as follows

$$GOx(FAD) + Glucose + O_2 \rightarrow GOx(FADH_2) + Gluconolactone + H_2O_2 \quad \text{(Eq. 1)}$$

$$GOx(FADH_2) + 2[Lu(III)Pc_2] + H_2O_2 \rightarrow GOx(FAD) + 2[Lu(II)Pc_2] + O_2 + 2H^+ \quad \text{(Eq. 2)}$$

$$2[Lu(II)Pc_2] + 2H^+ \rightarrow 2[Lu(III)Pc_2] + 2e^- \quad \text{(Eq. 3)}$$

Glucose is transferred from bulk solution to the PAA-rGO/VS-PANI/$LuPc_2$/GOx-MFH biosensor through diffusion. The enzyme GOx(FAD) in the presence of the natural co-substrate O_2, converts glucose to gluconic acid and O_2 to H_2O_2. The reduced GOx($FADH_2$) will be reoxidized by Lu(III)Pc_2 which exists in the MFH. The reduced mediator, Lu(II)Pc_2 which remains intact inside the MFH, is completely oxidized back to Lu(III)Pc_2 when the anodic potential is applied, resulting in high currents. A similar mechanism was reported for the electrochemical determination of glucose by GOx and the mediator by the Mn(III)-M(IV) tetra(o-aminophenyl)rphyrin couple (Rishpon et al., 1991), cobalt(II) phthalocyanine–cobalt(II) tetra(5-phenoxy-10,15,20-triphenylporphyrin), (CoPc–$(CoTPP)_4$) pentamer (Ozoemena and Nyokong, 2006) and Au-ME-CoTCAPc SAM (Mashazi et al., 2006). However electrocatalytic oxidation of glucose at PAA/VS-PANI/$LuPc_2$/GOx-MFH and PAA-rGO/$LuPc_2$/GOx-MFH showed only a marginal increase in the anodic current value (SI-5). This confirms the importance of individual component (PAA, rGO, and VS-PANI) as interconnected network in the hydrogel. To ascertain the importance of $LuPc_2$ and GOx in MFH for glucose sensing, a similar MFH biosensor was fabricated without loading $LuPc_2$ and GOx immobilization. MFH biosensor in the absence of GOx does not show glucose response in the applied potential region. However, for MFH biosensor in the absence of $LuPc_2$, the oxidation glucose response current was feeble (figures not shown). This further ensures the significance of combined presence of $LuPc_2$ and GOx in MFH for good electrochemical glucose determination.

3.8. Amperometric response of glucose at PAA-rGO/VS-PANI/$LuPc_2$/GOx-MFH biosensor

To demonstrate the functioning of PAA-rGO/VS-PANI/$LuPc_2$/GOx-MFH as a potential glucose biosensor, amperometric measurements were recorded for varied glucose concentration as shown in Fig 4B. Optimization of parameters for recording amperometric measurements were presented in SI-6. PAA-rGO/VS-PANI/$LuPc_2$/GOx-MFH biosensor was kept at +0.3 V in 0.1M PBS (pH 7.0). The bioelectrocatalytic current response for the successive additions of 1 mM glucose was monitored amperometrically under stirred condition. The PAA-rGO/VS-PANI/$LuPc_2$/GOx-MFH biosensor showed a rapid response to the changes in glucose concentration and the steady-state response current reached within 1s. The response time is much lower than PANI incorporated silica particles (Manesh et al., 2010), MWNT-g–SPAN-NW GOx based biosensors (Lee et al., 2010), GOx/PtNP/PAni hydrogel/Pt (Zhai et al., 2013), and GOx/GNp/CS/GOx/GNp/PAA/Pt (Wu et al., 2007). The reduced amperometric response time observed here is attributed to the faster diffusion of

glucose into the porous three-dimensional PAA-rGO/VS-PANI MFH. The rapid response to glucose was also achieved due to the existence of $LuPc_2$ that transfers electrons at a fast pace from GOx to MFH (Koide and Yokoyama, 1999; Dervisevic et al., 2014). The amperometric *i–t* response current of the biosensor is linear in the range of 2–12 mM concentration of glucose (R^2 = 0.9903) as shown in Fig. 4B(Inset, line (a)) with the sensitivity of 15.31 μA mM^{-1} cm^{-2} calculated from the slope of the calibration plot. The sensitivity is higher than those of 5.2 μA cm^{-2} mM^{-1} for GOD immobilized in an osmium-based three-dimensional redox hydrogel (Ohara et al., 1994), 1.7 μA cm^{-2} mM^{-1} for GOD formed upon cross-linking with the copolymer hydrogels (Lumley-Woodyear et al., 1995). To illustrate the importance of $LuPc_2$ and GOx in the fabrication of glucose biosensor, the amperometric *i-t* response for glucose was also observed for electrodes PAA-rGO/VS-PANI/$LuPc_2$-MFH and pristine PAA-rGO/VS-PANI-MFH (both fabricated without GOx). Typically, the electrodes exhibited a linear range from 2-5 mM (PAA-rGO/VS-PANI/$LuPc_2$-MFH) as shown in Fig. 4B(Inset, line (b)) and 1-3 mM (pristine PAA-rGO/VS-PANI-MFH) as shown in Fig. 4B(Inset, line (c)) of glucose respectively. The linear range of glucose detection for pristine PAA-rGO/VS-PANI-MFH and PAA-rGO/VS-PANI/$LuPc_2$-MFH are relatively lower than PAA-rGO/VS-PANI/$LuPc_2$/GOx-MFH biosensor. Furthermore, the sensitivity of PAA-rGO/VS-PANI/$LuPc_2$-MFH (0.912 μA mM^{-1} cm^{-2}) and prisitine PAA-rGO/VS-PANI-MFH (0.455 μA mM^{-1} cm^{-2}) are ~16.8 and ~33.6 times lower than PAA-rGO/VS-PANI/$LuPc_2$/GOx-MFH biosensor. The smaller linear range along with lowered sensitivity value in the case of PAA-rGO/VS-PANI/$LuPc_2$-MFH and prisitine PAA-rGO/VS-PANI-MFH might be due the blockage of pores in the hydrogel structures by the oxidised products of glucose which in-turn hampered the diffusion of glucose molecules to the electrode surface. However, the obtained longer linear response of PAA-rGO/VS-PANI/$LuPc_2$/GOx-MFH biosensor (2-12 mM) to glucose is suitable for glucose detection in human blood samples (normal glucose range in human blood is 4.4–6.6 mM). The wide linear range with high sensitivity of PAA-rGO/VS-PANI/$LuPc_2$/GOx-MFH biosensor for the amperometric detection of glucose may be due to the following facts. The porous three dimensional PAA-rGO/VS-PANI MFH matrices offer low diffusional resistance to glucose and hence reduces the mass transport barrier. rGO and VS-PANI as interconnected network within hydrogel provide electronic conductivity to achieve fast electron transport. PAA based hydrogel craft favorable environment for loading $LuPc_2$ and GOx enzyme immobilization (Zhao et al., 2013). The results obtained from the amperometric current response of glucose at PAA-rGO/VS-PANI/$LuPc_2$-MFH and pristine PAA-rGO/VS-PANI-MFH electrodes

illustrate that GOx plays the key component in the detection of glucose and $LuPc_2$ effectively transfers electrons from GOx to the electronically conducting hydrogel matrix.

The apparent Michaelis–Menten constant (K_M) was calculated as 17.05 mM using the slope and intercept values from Lineweaver–Burk plot for PAA-rGO/VS-PANI/$LuPc_2$/GOx-MFH biosensor (Iwuoha and Smyth, 1997). The K_M value obtained for this biosensor is higher than other GOx-mediator based glucose sensors (Ghica and Brett, 2005). The high value of K_M informs that the GOx in the PAA-rGO/VS-PANI/$LuPc_2$/GOx-MFH biosensor possesses higher affinity for glucose. The limit of detection (LoD) for glucose at PAA-rGO/VS-PANI/$LuPc_2$/GOx-MFH biosensor was calculated as 25 μM (signal to noise ratio = 3). The detection limit is estimated as three times of the standard deviation of the background. The LoD value was lower than Ru mediator attached PVPAA copolymer/GOx biosensor (Deng, et al, 2014). In enzymless detection of glucose a LoD in the nano mole range has been found for Cu/3D graphene hybrid-based electrode (Hussain et al., 2015).

The analytical performance of the proposed sensor are compared with similar enzyme/mediator based glucose biosensors and presented in Table 1. From the Table 1 values it is understood that the proposed PAA-rGO/VS-PANI/$LuPc_2$/GOx-MFH biosensor exhibits wide linear range response to glucose, high sensitivity and low LoD.

3.9. Repeatability, Reproducibility and stability of PAA-rGO/VS-PANI/$LuPc_2$/GOx-MFH biosensor

Different aspects concerning the utility of PAA-rGO/VS-PANI/$LuPc_2$/GOx-MFH as sensible glucose biosensor were evaluated. The repeatability of PAA-rGO/VS-PANI/$LuPc_2$/GOx-MFH as sensible glucose biosensor was tested through amperometric measurements for two different concentrations of glucose, 4 mM and 6 mM (SI-7). Seven repetitive measurements of a single PAA-rGO/VS-PANI/$LuPc_2$/GOx-MFH biosensor (washed with 0.1M PBS between individual measurements) yielded a relative standard deviation (RSD) value of 6.1% (4 mM) and 6.5% (6 mM) of glucose. To demonstrate the stability of fabricated PAA-rGO/VS-PANI/$LuPc_2$/GOx-MFH biosensor, amperometric response to 4 mM glucose solution was periodically registered for a period of 3 months keeping the electrodes stored at 4 °C refrigerated condition. It has been found that the PAA-rGO/VS-PANI/$LuPc_2$/GOx-MFH biosensor retained > 98% of current response which indicates that the functioning of GOx well protected within the new MFH without leaching under ideal conditions. The leaching effect of $LuPc_2$ from the fabricated PAA-rGO/VS-PANI/$LuPc_2$-MFH was investigated by

recording UV-visible spectrum before and after immersion into 0.1M PBS for a time period of 30 minutes (time taken to record amperometry). From the characteristic B and Q band absorption peaks of $LuPc_2$ it is confirmed that there is no leaching of $LuPc_2$ from PAA-rGO/VS-PANI/$LuPc_2$-MFH electrode. This may be due to the π-π interaction between the rGO, VS-PANI with double ducker $LuPc_2$ (Fukuda et al., 2012). The reproducibility of PAA-rGO/VS-PANI/$LuPc_2$/GOx-MFH biosensor was estimated with ten similarly fabricated sensor assemblies. The results revealed that the biosensor has a satisfactory reproducibility (RSD = 2.2%, n = 10). Under the applied potential of +0.3 V, the addition of interfering substances such as ascorbic acid and uric acid hardly affects the amperometric response current of glucose (4 mM) (SI-8). With three repetitive measurements of glucose (4 mM) along-with interfering substances in a single PAA-rGO/VS-PANI/$LuPc_2$/GOx-MFH biosensor, the coefficient of variation (COV) was found to be 10.03%. Also the COV was calculated for the reproducibility test results of glucose (4 mM) in the presence of interference and was found to be 11.36% (n=5). This shows that PAA-rGO/VS-PANI/$LuPc_2$-MFH biosensor exhibit selective detection of glucose even in the presence of electrochemically active substances.

3.10. Glucose determination in real samples at PAA-rGO/VS-PANI/$LuPc_2$/GOx-MFH biosensor

To illustrate the feasibility of PAA-rGO/VS-PANI/$LuPc_2$/GOx-MFH as potential biosensor in industrial as well in clinical diagnosis, real sample analysis was carried out. In our work, commercial glucose samples and human serum obtained from Biomolecular Sciences Research Centre at Sheffield Hallam University were suitably diluted using 0.1 M PBS (pH 7.0) to obtain required concentration sample solutions. A continuous amperometry was recorded for varied additions of real samples under identical experimental conditions as similar to Fig. 4B. PAA-rGO/VS-PANI/$LuPc_2$/GOx-MFH biosensor exhibited response to all the real samples added. The data obtained from analysis are summarized in SI-9. The results obtained are satisfactory with an error percentage of +3.0. The satisfactory results demonstrate good practical applicability of the proposed biosensor.

4. Conclusions

In this work, we demonstrate the synthesis of multifunctional conducting polyacrylic acid (PAA) hydrogel (MFH) integrated with reduced grapheme oxide (rGO) and vinyl substituted polyaniline (VS-PANI) (PAA-rGO/VS-PANI-MFH). A redox mediator based glucose

biosensor was constructed by loading lutetium phthalocyanine ($LuPc_2$) and glucose oxidase (GOx) into PAA-rGO/VS-PANI-MFH matrix (PAA-rGO/VS-PANI/$LuPc_2$/GOx-MFH). The structural stability and hierarchical porosity of PAA-rGO/VS-PANI-MFH resulted in large surface area for GOx immobilization. The high electrical conductivity is achieved through interconnected VS-PANI network for rapid mass/charge transport. $LuPc_2$ functions as an excellent redox mediator and reduces the amperometric glucose detection potential to +0.3 V. The present work demonstrates that the multi-components (rGO,VS-PANI, and $LuPc_2$) have synergistic influences on the performance of biosensor. The PAA-rGO/VS-PANI/$LuPc_2$/GOx-MFH biosensor exhibits wide linear range and high sensitivity to glucose with a low detection limit. PAA-rGO/VS-PANI/$LuPc_2$/GOx-MFH could be effectively used as an electrochemical biosensor in industrial as well clinical diagnosis. Further, the MFH provides scope for loading of other redox enzymes to fabricate high performance biosensors.

5. Acknowledgements

Hadi Al-Sagur acknowledges the financial support provided for his PhD study from the Ministry of Higher Education and Scientific Research (MOHESR) and the College of Medicine/Thi Qar University in Iraq. Support from MERI technical staff is gratefully acknowledged.

6. Supporting informations are available for this paper

References

Arunbabu, D., Shahsavan, H., Zhang, W., Zhao, B., 2013. J. Phys. Chem. B, 117, 441–449

Åsberg, P., Inganäs, O., 2003. Biosens. Bioelectron. 19, 199–207.

Bai, H., Li, C., Wang, X., Shi, G., 2010. Chem. Commun. (Camb). 46, 2376–2378.

Barakat, M.A., Sahiner, N., 2008. J. Environ. Manage. 88, 955–961.

Barrera, C., Zhukov, I., Villagra, E., Bedioui, F., Páez, M.A., Costamagna, J., Zagal, J.H., 2006. J. Electroanal. Chem. 589, 212–218.

Basova, T., Jushina, I., Gürek, A.G., Ahsen, V., Ray, A.K., 2008. J. R. Soc. Interface 5, 801–

806.

Basova, T., Plyashkevich, V., Hassan, A., 2008. Surf. Sci. 602, 2368–2372.

Bhattacharjee, P., Paul, S., Banerjee, M., Patra, D., Banerjee, P., Ghoshal, N., Bandyopadhyay, A., Giri, A.K., 2013. Sci. Rep. 3, 2704.

Canadian Diabetes Association, 2008. Can. J. Diabetes 32, S1–S201.

Chen, C., Jiang, Y., Kan, J., 2006. Biosens. Bioelectron. 22, 639–643.

Claussen, J.C., Kumar, A., Jaroch, D.B., Khawaja, M.H., Hibbard, A.B., Porterfield, D.M., Fisher, T.S., 2012. Adv. Funct. Mater. 22, 3399–3405.

Crouch, E., Cowell, D.C. Hoskins, S. Pittson, R.W. Hart, J.P., 2005. Anal. Biochem. 347, 17-23

Deng, H., Liang, A. K., Gao, Z., 2014. Sens. Actu. B: Chem.. 191, 522–528.

Deng, H., Shen, W., Gao, Z., 2013. ChemPhysChem 14, 2343–2347

Dervisevic, M., Çevik, E., Şenel, M., 2014. Enz. Micro. Tech. 68, 69–76.

Dhodapkar, R., Borde, P., Nandy, T., 2009. Global NEST Journal. 11, 223-234.

Diabetes UK, Monday 15 June 2015; (https://www.diabetes.org.uk/About_us/News/39-million-people-now-living-with-diabetes/)

Ding, H., Zhong, M., Kim, Y.J., Pholpabu, P., Balasubramanian, A., Hui, C.M., He, H., Yang, H., Matyjaszewski, K., Bettinger, C.J., 2014. ACS Nano. 8, 4348–4357.

Ding, S.J., Chang, B.W., Wu, C.C., Lai, M.F., Chang, H.C., 2005. Anal. Chim. Acta 554, 43–51.

Dou, P., Liu, Z., Cao, Z., Zheng, J., Wang, C., Xu, X., 2016. J. Mater. Sci. 51,4274–4282.

Fukuda, T., Hata, K. and Ishikawa, N., 2012. J. Am. Chem. Soc. 134, 14698-14701.

Gaharwar, A.K., Peppas, N.A., Khademhosseini, A., 2014. Biotechnol. Bioeng. 111, 441–453.

Galanin, N.E., Shaposhnikov, G.P., 2012a. Russ. J. Gen. Chem. 82, 1734–1739.

1 Galanin, N.E., Shaposhnikov, G.P., 2012b. Russ. J. Org. Chem. 48, 851–857.

2 Garjonyte, R., Malinauskas, A., 1999. Sensors Actuators B Chem. 56, 85–92.

3 Ghica, M.E., Brett, C. M.A., 2005 Anal. Chim. Act. 532, 145–151.

4 Guo, H., He, W., Lu, Y., Zhang, X., 2015. Carbon N. Y. 92, 133–141.

5 Gurek, A.G., Ahsen, V., Luneau, D., and Pecaut, J., 2001. Inorg. Chem., 40, 4793-4797.

6 Hart, J.P., Wring, S.A., 1997. TrAC - Trends Anal. Chem. 16, 89–103.

7 Heller, A., 2006. Curr. Opin. Chem. Biol. 10, 664–672.

8 Horng, Y-Y., Hsu, Y-K., Ganguly, A., Chen, C-C., Chen, L-C., Chen, K-H., 2009.
9 Electrochem. Commun. 11, 850–853.

10 Hou, S.-F., Yang, K.-S., Fang, H.-Q. Chen, H.-Y., 1998. Talanta 47, 561-567.

11 Hua, L., Wu, X., Wang, R., 2012. Analyst. 137, 5716-5719.

12 Hussain, S., Akbar, K., Vikraman, D., Choi, D-C., Kim, S. J., An, K-S., Jung, S., Jung, J.,
13 2015. New J. Chem. 39, 7481-7487.

14 Ipek, Y., Dinçer, H., Koca, A., 2014. Sens. Act. B Chem. 193, 830–837.

15 Iwuoha, I.E., Smyth, M.R., 1997. Biosens. Bioelectron, 12, No. 1, 53-75.

16 Iza, M., Woerly, S., Danumah, C., Kaliaguine, S., Bousmina, M., 2000. Polymer 41, 5885–
17 5893.

18 Kadish, K.M., Nakanishi, T., Gürek, A., Ahsen, V., Yilmaz, I., 2001. J. Phys. Chem. B. 105,
19 9817–9821.

20 Katz, E. and W.I., 2003. Electroanal. 15, 913–947.

21 Koide, S., Yokoyama, K., 1999. J. Elect. Chem 468, 193–201.

22 Komathi, S., Gopalan, A. I., Lee, K.-P., 2009. Biosens. Bioelectron, 24, 10, 3131-3134.

23 Layek, R.K., Nandi, A.K., 2013. Polymer 54, 5087-5103.

24 Lee, K.P., Komathi, S., Nam, N.J., Gopalan, A.I., 2010. Microchem. J. 95, 74–79.

1 Lei, L., Xia, Z., Zhang, L., Zhang, Y., Zhong, L., 2016. Prog. Org. Coatings 97, 19–27.

2 Li, W., Zhao, H., Teasdale P.R., John, R., Zhang, S., 2002. React. .Fun. Poly. 52, 31–41.

3 Liu, J., Chen, G., Jiang, M., 2011. Macromolecules 44, 7682–7691.

4 Lumley-Woodyear, T., Rocca, P., Lindsay, J., Dror, Y., Freeman, A.,Heller, A., 1995. Anal.
5 Chem. 67 ,1332‑1338.

6 Manesh, K.M., Santhosh, P., Uthayakumar, S., Gopalan, A.I., Lee, K.P., 2010. Biosens.
7 Bioelectron. 25, 1579–1586.

8 Mani, V., Devasenathipathy, R., Chen, S.M., Gu, J.A., Huang, S.T., 2015. Renew. Energy 74,
9 867–874.

10 Mashazi, P.N., Ozoemena, K.I., Nyokong, T., 2006. Electrochim. Acta 52, 177–186.

11 Nabid, M.R., Sedghi, R., Jamaat, P.R., Safari, N., Entezami, A.A., 2007. Appl. Catal. A Gen.
12 328, 52–57.

13 Nath, B.C., Gogoi, B., Boruah, M., Sharma, S., Khannam, M., Ahmed, G.A., Dolui, S.K.,
14 2014. Electrochim. Acta 146, 106–111.

15 Nekelson, F., Monobe, H., Shiro, M., Shimizu, Y., 2007. J. Mater. Chem. 17, 2607.

16 Ohara, T.J., Rajagopalan, R., Heller, A., 1994. Anal. Chem. 66, 2451‑2457.

17 Ozoemena, K.I., Nyokong, T., 2006. Electroch. Act. 51, 5131–5136.

18 Ozoemena, K.I., Zhao, Z., Nyokong, T., 2005. Electrochem. commun. 7, 679–684.

19 Pal, C., Cammidge, a N., Cook, M.J., Sosa-Sanchez, J.L., Sharma, a K., Ray, a K., 2011. J.
20 R. Soc. Interface 74, 2848–2850.

21 Pan, L., Yu, G., Zhai, D., Lee, H.R., Zhao, W., Liu, N., Wang, H., Tee, B.C.-K., Shi, Y., Cui,
22 Y., Bao, Z., 2012. Proc. Natl. Acad. Sci. U. S. A. 109, 9287–92.

23 Pei, R., Cheng, Z., Wang, E., Yang, X., 2001. Biosens. Bioelectron. 16, 355–361

24 Pereira-Rodrigues, N., Albin, V., Koudelka-Hep, M., Auger, V., Pailleret, A., Bedioui, F.,
25 2002. 4, 922–927.

Pushkarev, V.E., Tolbin, A.Y., Zhurkin, F.E., Borisova, N.E., Trashin, S.A., Tomilova, L.G., Zefirov, N.S., 2012. Chem. - A Eur. J. 18, 9046–9055.

Rahman, M.M., Ahammad, A.J.S., Jin, J.H., Ahn, S.J., Lee, J.J., 2010. Sensors 10, 4855–4886.

Ren, Q., Feng, L., Fan., R., Ge, X., Sun, Y., 2016. Mat. Sci. Eng. C 68, 308–316.

Ren, X., Chen, D., Meng, X., Tang, F., Du, A., Zhang, L., 2009. Colloids Surfaces B Biointerfaces 72, 188–192.

Rishpon J., Rosen-Margalit I., Harth R., Ozer D., Bettelheim A., 1991. J. Electroanal. Chem. 307, 293-298

Saravanan, S., Anantharaman, M.R., Venkatachalam, S., 2006. Mater. Sci. Eng. B Solid-State Mater. Adv. Technol. 135, 113–119.

Schuit, F., Huypens, P., Heimberg, H., Pipeleers, D., 2001. Diabetes 50, 1–11.

Sezgin, N., Balkaya, N., 2015. Water Treat. 3994, 1–15.

Siswana, M.P., Ozoemena, K.I., Nyokong, T., 2006. Electrochim. Acta 52, 114–122.

Soomro, R. A., Ibupoto, Z. H., Sirajuddin, Abro, M. I., Willander, M., 2015. Sens. Act. B: Chem. 209, 966–974.

Thirumalraj, B., Palanisamy, S., Chen, S.-M., Yang, C.-Y., Periakaruppan, P., Lou, B.-S., 2015. RSC Adv. 5, 77651–77657.

Toghill, K.E., Compton, R.G., 2010. J. Electrochem. Sci. 5, 1246–1301.

Unnikrishnan, B., Palanisamy, S., Chen, S.M., 2013. Biosens. Bioelectron. 39, 70–75.

Wang, H.-C., Lee, A.-R., 2015. J. Food Drug Anal. 23, 191–200.

Wang, J, 2001, Electroanal. 13, 983-988.

Wang, K., Xu, J.J., Chen, H.Y., 2005. Biosens. Bioelectron. 20, 1388–1396.

Wang, K., Zhang, X., Li, C., Zhang, H., Sun, X., Xu, N., Ma, Y., 2014. J. Mater. Chem. A 2, 19726–19732.

Wang, Z., Liu, S., Wu, P., Cai, C., 2009. Anal. Chem., 81 , 1638–1645.

Wild S, Roglic G, Green A, Sicree R, King H, 2004, Diabetes Care, 27, 1047–1053.

Worsley, M.A., Kucheyev, S.O., Mason, H.E., Merrill, M.D., Mayer, B.P., Lewicki, J., Valdez, C. a., Suss, M.E., Stadermann, M., Pauzauskie, P.J., Satcher, J.H., Biener, J., Baumann, T.F., 2012. Chem. Commun. 48, 8428–8430.

Wu, B.Y., Hou, S.H., Yin, F., Li, J., Zhao, Z.X., Huang, J.D., Chen, Q., 2007. Biosens. Bioelectron. 22, 838–844.

Wu, C., Sun, H., Li, Y., Liu, X., Du, X., Wang, X., Xu, P., 2015. Biosens. Bioelectron. 66, 350–355.

Ye, J.S., Wen, Y., De Zhang, W., Cui, H.F., Xu, G.Q., Sheu, F.S., 2005. Electroanalysis 17, 89–96.

Zen, J.M., Senthil Kumar, A., Chung, C.R., 2003. Anal. Chem. 75, 2703–2709.

Zhai, D., Liu, B., Shi, Y., Pan, L., Wang, Y., Li, W., Zhang, R., Yu, G., 2013. ACS Nano 7, 3540–3546.

Zhang, L., Zhou, C., Luo, J., Long, Y., Wang, C., Yu, T., 2015. J. Mater. Chem. B Mater. Biol. Med. 3, 1116–1124.

Zhao, Y., Liu, B., Pan, L., Yu, G., 2013. Energy Environ. Sci. 6, 2856.

Zheng, H., Xue, H., Zhang, Y., Shen, Z., 2002, Biosens. Bioelectron., 17, 541‑545.

Zheng, W., Wang, B.-B., Lai, J.-C., Wan, C.-Z., Lu, X.-R., Li, C.-H., You, X.-Z., 2015. J. Mater. Chem. C 3, 3072–3080.

Zhou, M., Shang, L., Li, B., Huang, L., Dong, S., 2008. Biosens. Bioelectron. 24, 442-447.

Zhu, Z., Garcia-Gancedo, L., Flewitt, A.J., Xie, H., Moussy, F., Milne, W.I., 2012. Sensors (Basel). 12, 5996–6022.

Zugle, R., Antunes, E., Khene, S., Nyokong, T., 2012. Polyhedron 33, 74–81.

1

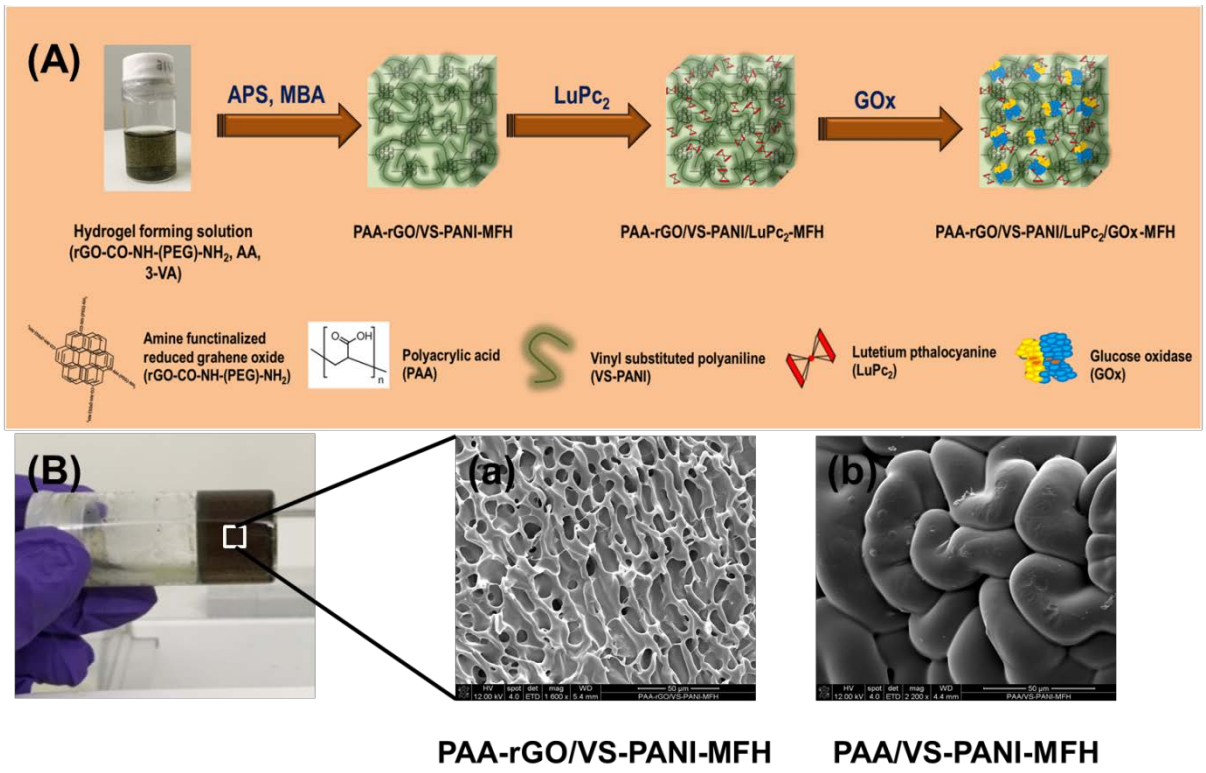

Fig. 1. (A) Schematic representation of the formation of PAA-rGO/VS-PANI/$LuPc_2$/GOx-MFH; (B) SEM images of (a) PAA-rGO/VS-PANI-MFH, (b) PAA/VS-PANI-MFH

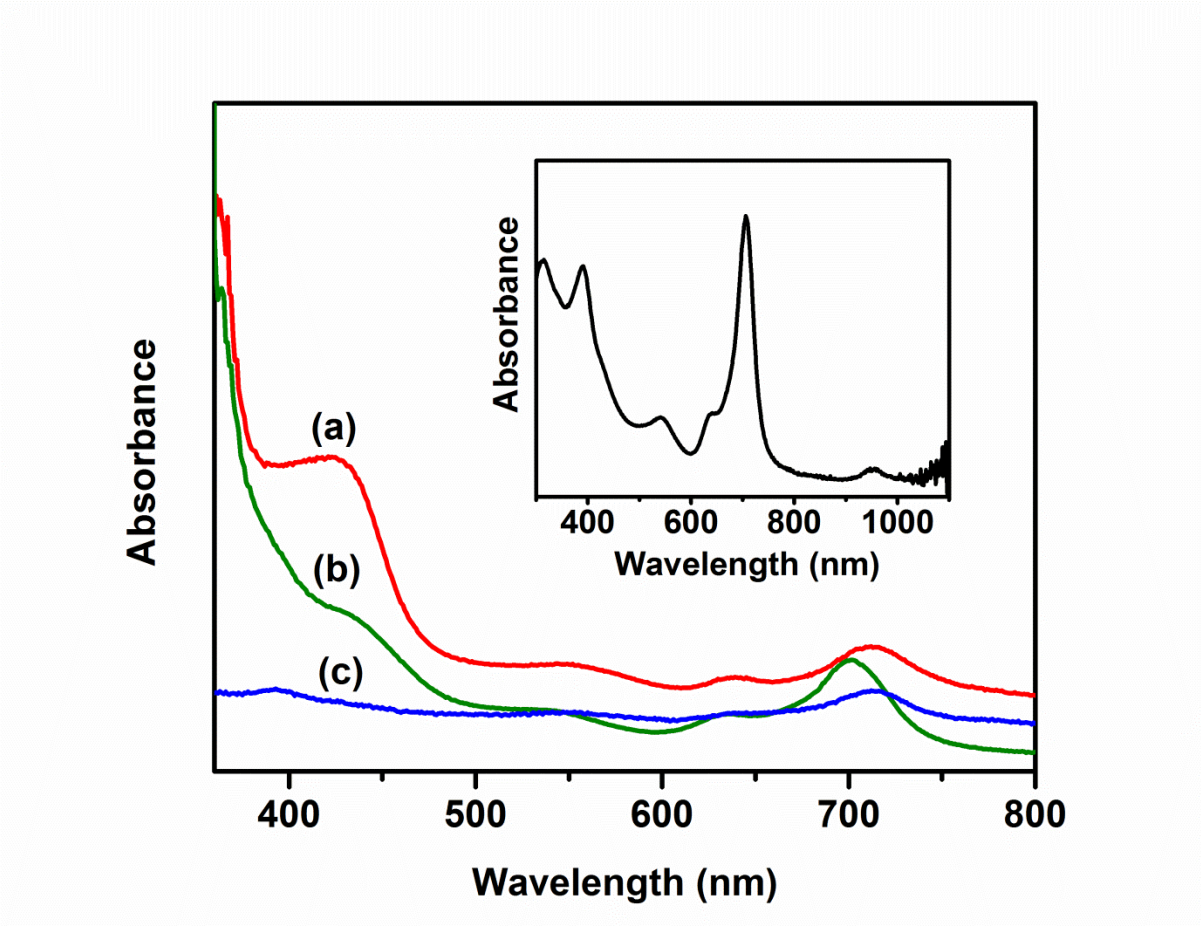

Fig. 2. UV-visible spectrum of (a) PAA-rGO/VS-PANI/$LuPc_2$-MFH, (b) PAA/VS-PANI/$LuPc_2$-MFH, (c) PAA-rGO/$LuPc_2$ -MFH. Inset UV-visible spectrum of $LuPc_2$ film

1

2

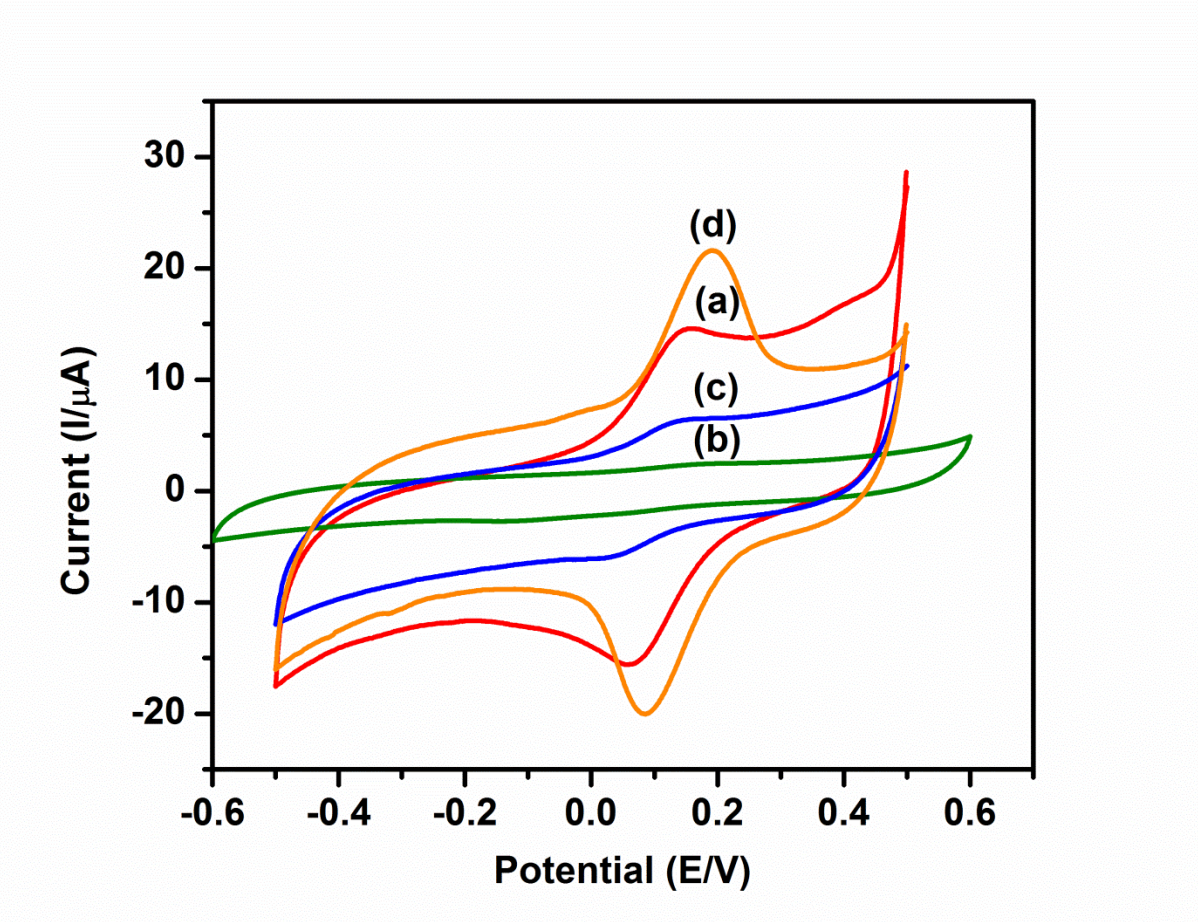

Fig. 3. Cyclic voltammogram of (a) PAA-rGO/VS-PANI/$LuPc_2$/GOx-MFH, (b) PAA/VS-PANI/$LuPc_2$/GOx-MFH, (c) PAA-rGO/$LuPc_2$/GOx-MFH, (d) PAA-rGO/$LuPc_2$-MFH recorded in 5 mM Potassium ferro/ferri cyanide solution containing 0.1M NaCl; scan rate = 25 mV/s

1

2

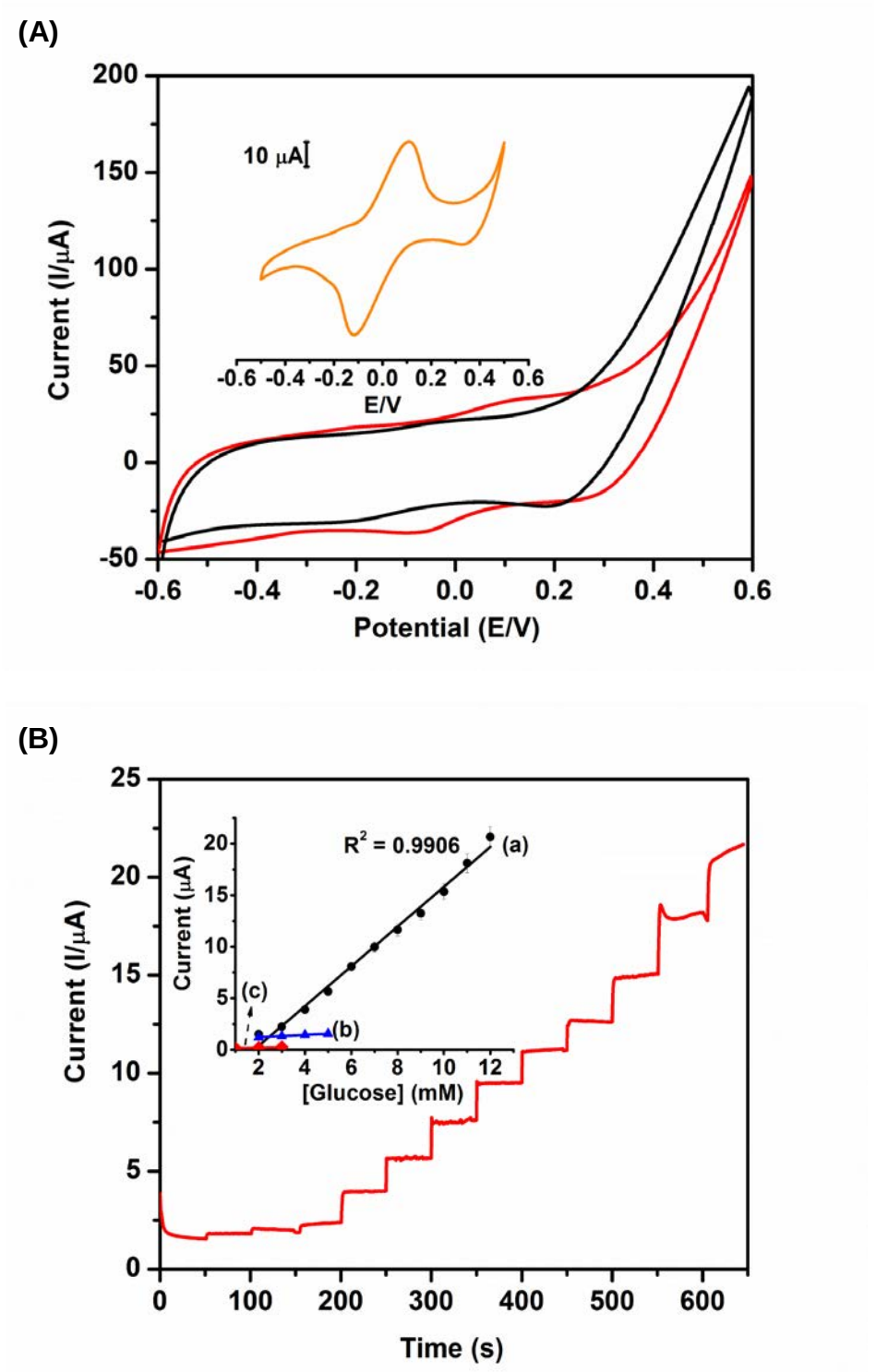

Fig. 4. (A) Cyclic voltammogram of PAA-rGO/VS-PANI/$LuPc_2$/GOx-MFH (red line) 0 mM glucose and (black line) 4 mM glucose in 0.1M PBS (pH 7.0). Inset Cyclic voltammogram of PAA-rGO/VS-PANI/$LuPc_2$-MFH in 0.1M PBS (pH 7.0); (B) Amperometry of PAA-rGO/VS-PANI/$LuPc_2$/GOx-MFH for successive addition of glucose in 0.1M PBS (pH 7.0). Inset: calibration plot peak current versus [glucose].

1

Table 1. Comparison of analytical performance of some glucose biosensors

Electrode	Response time (s)	Iinear range (mM)	Sensitivity ($\mu A\ mM^{-1}\ cm^{-2}$)	LOD (μM)	Ref.
Au-MPS-OsPVP-GOx	5	0.1–10	-	50	(Hou et al., 1998)
SPCE/CoPC/GOD	60	0.2–5	1.12	-	(Crouch et al., 2005)
GCE–CoPc–$(CoTPP)_4$–GOx	~5	upto 11	0.024	10	(Ozoemena and Nyokong, 2006)
{GOx/Au-(SH)PANI-g-MWNT}*n*/ITO	~8	1–9	3.97	0.06	(Komathi et al., 2009)
GOx-nanoPANi/Pt	3	0.01-5.5	97.18±4.62	0.3±0.1	(Wang et al., 2009)
GOx-PANI nanowire	10	0–8	2.5	0.05	(Horng et al., 2009)
GOD/ERGO/PLL/GC	-	0.25 - 5	-	-	(Hua et al., 2012)
Nafion-GOx-ordered mesoporous carbon	9±1	5-15	0.053	156.52	(Zhou et al., 2008)
Os(2,2′bpy)2-RP/GOx	<5	0-10	16.5	-	(Deng et al., 2013)
poly(GMA-co-VFc)-GOx	1	1-17	0.27	33	Dervisevic et al., 2014
Au/CA/(GOx/TFGn)n	6	1-13 mM	19.9	-	(Ren et al., 2016)
Hedgehog-like NiO nanostructures	-	0.1–5.0 μM	1052.8	1.2	(Soomro et al., 2015)
PAA-rGO/VS-PANI/$LuPc_2$/GOx-MFH	~1	2-12	15.31	25	Our present work